AN INCREASE IN THE FAINT RED GALAXY POPULATION IN MASSIVE CLUSTERS SINCE $z \sim 0.5$

J. P. STOTT,[1] IAN SMAIL,[1] A. C. EDGE,[1] H. EBELING,[2] G. P. SMITH,[3] J.-P. KNEIB,[4] AND K. A. PIMBBLET[5]

ABSTRACT

We compare the luminosity functions for red galaxies lying on the rest-frame $(U - V)$ color-magnitude sequence in a homogeneous sample of 10 X-ray-luminous clusters from the MACS survey at $z \sim 0.5$ to a similarly selected X-ray cluster sample at $z \sim 0.1$. We exploit deep *Hubble Space Telescope* ACS imaging in the F555W and F814W passbands of the central 1.2 Mpc diameter regions of the distant clusters to measure precise colors for the galaxies in these regions and statistically correct for contamination by field galaxies using observations of blank fields. We apply an identical analysis to ground-based photometry of the $z \sim 0.1$ sample. This comparison demonstrates that the number of faint, $M_V \sim -19$, red galaxies relative to the bright population seen in the central regions of massive clusters has roughly doubled over the 4 Gyr between $z \sim 0.5$ and $z \sim 0.1$. We quantify this difference by measuring the dwarf-giant ratio on the red sequence, which increases by a factor of at least 2.2 ± 0.4 since $z \sim 0.5$. This is consistent with the idea that many faint, blue, star-forming galaxies in high-density environments are transforming onto the red sequence in the last half of the Hubble time.

Subject headings: galaxies: clusters: general — galaxies: evolution — galaxies: luminosity function, mass function

1. INTRODUCTION

Recent studies have precisely quantified the variation in the photometrically classified galaxy population as a function of environment at low redshifts (Hogg et al. 2004). These studies separate galaxies into systems that are red and passive or those that are blue and star-forming, and find that the proportion of the latter decreases in higher density regions in the local universe (Baldry et al. 2006). The identification of the physical process responsible for this trend is still contentious, in part because it is likely that a number of processes contribute in different environments, at different epochs and acting on galaxies of different luminosities/masses. The presence of a range of potential evolutionary pathways linking star-forming and passive galaxies may be reflected in the diversity of star formation histories derived for passive early-type galaxies. While the formation of luminous early-type galaxies in clusters has been interpreted in terms of a narrow range in star formation histories (Bower et al. 1992; Aragon-Salamanca et al. 1993; van Dokkum et al. 1998; Stanford et al. 1998), there is evidence of much more variety in lower luminosity systems (see Ferguson & Binggeli 1994 for a review). Several lines of evidence illustrate this, for example Poggianti et al. (2001) find a broad range in ages but a slight decrease in age for fainter dwarf galaxies in the Coma Cluster. Smail et al. (2001) reached a similar conclusion for the luminosity-weighted ages of low-luminosity early-type galaxies in the $z = 0.18$ cluster Abell 2218. An even wider variety is found in much lower luminosity systems, Grebel (1999) finds that star formation timescales and ages vary significantly for the local group dwarf ellipticals. Indeed, this same effect may underlie the varying morphological mix seen in the passive galaxy populations in clus-

ters, where there is a claim of a deficit of early-type disk galaxies (predominantly S0) in distant clusters (Dressler et al. 1997). Thus it appears that passive galaxies may be formed via a number of different processes and that the mixed nature of the population may be most easily discerned at the lowest luminosities.

These different pathways may also result in a changing passive galaxy population in clusters at different redshifts. The most fundamental measure of the transformational processes forming passive galaxies in high-density regions is to look at the build up of the luminosity function of this population. De Lucia et al. (2004) therefore investigated this scenario by measuring the color-magnitude relation in four optically selected $z \sim 0.75$ clusters and comparing these to the nearby Coma Cluster. They find that the high-redshift clusters exhibit a deficiency in low-luminosity red galaxies compared to Coma. Similarly, Kodama et al. (2004) found a deficit of red-sequence galaxies when looking at $z \sim 1$ high-density regions in the Subaru/*XMM-Newton* Deep Survey. This leads them to conclude that many faint red galaxies in clusters have only moved onto the red sequence since $z \sim 0.75$ (see also De Lucia et al. 2007). This result is controversial as Andreon (2006) claims there is no evidence for this red-sequence build-up when comparing the luminosity function of a cluster at $z = 0.831$ to those of local clusters.

In this paper we aim to test these results by comparing the evolution in the luminosity function of galaxies on the red sequence in two well-defined samples of X-ray-selected clusters at $z \sim 0.5$ and $z \sim 0.1$. We employ *Hubble Space Telescope* (*HST*) optical imaging of 10 $z \sim 0.5$ X-ray-luminous clusters and compare these to a similar sample at $z \sim 0.1$ to examine evolution in the faint end of the red-sequence luminosity function. We adopt a ΛCDM cosmology ($\Omega_M = 0.3$, $\Omega_{\rm vac} = 0.7$, and $H_0 = 70$ km s^{-1} Mpc^{-1}) in which the look-back times to $z = 0.13$ and 0.54 are 1.6 and 5.3 Gyr and the angular scales are such that $1''$ corresponds to 2.3 and 6.4 kpc, respectively. An AB magnitude system is used throughout this paper.

2. OBSERVATIONS AND REDUCTION

Our analysis employs rest-frame optical imaging of two cluster samples at $z \sim 0.1$ and $z \sim 0.5$. The $z \sim 0.5$ sample are

[1] Institute for Computational Cosmology, Department of Physics, Durham University, Durham DH1 3LE, UK; j.p.stott@durham.ac.uk.
[2] Institute for Astronomy, Honolulu, HI 96822.
[3] School of Physics and Astronomy, University of Birmingham, Edgbaston, Birmingham B15 2TT, UK.
[4] Laboratoire d'Astrophysique de Marseille, Marseille Cedex 12, France.
[5] Department of Physics, University of Queensland, Brisbane QLD 4072, Australia.

STOT ET AL.

TABLE 1
DETAILS OF THE CLUSTER SAMPLES USED IN OUR ANALYSIS

Cluster	R.A. (J2000.0)	Decl. (J2000.0)	z	L_X (10^{44} ergs s^{-1})	N_{red}[a]	DGR
MACS $z \sim 0.5$ Sample						
MACS J0025.4−1222	00 25 15.84	−12 19 44	0.478	12.4	168 ± 13	1.56 ± 0.35
MACS J0257.6−2209	02 57 07.96	−23 26 08	0.504	15.4	157 ± 13	1.47 ± 0.34
MACS J0647.7+7015	06 47 51.45	+70 15 04	0.584	21.7	183 ± 14	1.39 ± 0.29
MACS J0717.5+3745	07 17 31.83	+37 45 05	0.548	27.4	321 ± 18	1.25 ± 0.20
MACS J0744.8+3927	07 44 51.98	+39 27 35	0.686	25.9	173 ± 13	1.00 ± 0.22
MACS J0911.2+1746	09 11 10.23	+17 46 38	0.506	13.2	169 ± 13	1.54 ± 0.34
MACS J1149.5+2223	11 49 34.81	+22 24 13	0.544	17.3	266 ± 16	1.43 ± 0.25
MACS J1423.8+2404	14 23 47.95	+24 04 59	0.544	15.0	155 ± 13	1.11 ± 0.25
MACS J2129.4−0741	21 29 25.38	−07 41 26	0.570	16.4	194 ± 14	1.27 ± 0.26
MACS J2214.9−1359	22 14 56.51	−14 00 17	0.495	17.0	215 ± 15	1.25 ± 0.24
LARCS $z \sim 0.1$ Sample						
Abell 22	00 20 38.64	−25 43 19	0.142	5.3	220 ± 21	2.55 ± 0.64
Abell 550	05 52 51.84	−21 03 54	0.099	7.1	277 ± 22	2.05 ± 0.43
Abell 1084	10 44 30.72	−07 05 02	0.132	7.4	111 ± 18	4.00 ± 1.79
Abell 1285	11 30 20.64	−14 34 30	0.106	5.45	391 ± 25	2.94 ± 0.53
Abell 1437	12 00 25.44	+03 21 04	0.134	7.7	376 ± 25	2.04 ± 0.35
Abell 1650	12 58 41.76	−01 45 22	0.084	7.8	182 ± 20	3.00 ± 0.88
Abell 1651	12 59 24.00	−04 11 20	0.085	8.3	232 ± 21	4.52 ± 1.24
Abell 1664	13 03 44.16	−24 15 22	0.128	5.34	127 ± 18	2.49 ± 0.91
Abell 2055	15 18 41.28	+06 12 40	0.102	4.8	201 ± 21	4.54 ± 1.37
Abell 3888	22 34 32.88	−37 43 59	0.153	14.5	124 ± 19	1.89 ± 0.68
Additional Clusters						
Cl J0152−1357......................................	01 52 43.91	−13 57 21	0.831	5.0	276 ± 17	0.77 ± 0.14
MACS J0451.9+0006	04 51 54.63	+00 06 18	0.430	10.4	179 ± 14[b]	1.41 ± 0.30
MACS J0712.3+5931	07 12 20.45	+59 32 20	0.328	6.8	90 ± 10[b]	1.63 ± 0.44
Cl J1226.9+3332....................................	12 26 58.13	+33 32 49	0.890	20.0	232 ± 15	1.16 ± 0.22
Abell 1703	13 15 00.70	+51 49 10	0.258	8.7	94 ± 10[c]	3.48 ± 1.13
MACS J1354.6+7715	13 54 19.71	+77 15 26	0.397	8.2	156 ± 13[c]	1.66 ± 0.37

NOTES.—Units of right ascension are hours, minutes, and seconds, and units of declination are degrees, arcminutes, and arcseconds. The limited radius of MACS 1354 is due to size of ACS image and flaring on the image from a bright star. The LARCS redshifts are from Pimbblet et al. (2006). MACS redshifts come from H. Ebeling et al. (2007).
[a] Number of galaxies on the red sequence down to $M_V = -17.75$ within a 600 kpc radius of cluster center, except when otherwise noted.
[b] Number of galaxies on the red sequence down to $M_V = -17.75$ within a 400 kpc radius of cluster center.
[c] Number of galaxies on the red sequence down to $M_V = -17.75$ within a 300 kpc radius of cluster center.

selected from the Massive Cluster Survey (MACS; Ebeling et al. 2001). MACS is a survey of distant X-ray-luminous ($L_X > 10^{44}$ ergs s^{-1}), and therefore massive, galaxy clusters selected from the *ROSAT* All-Sky Survey. The 10 clusters in this sample, along with a further two for which archival *HST* observations exist, are the 12 most distant clusters, $z \sim 0.5$–0.7, from MACS and all have X-ray luminosities of $L(0.1$–2.4 KeV$) > 15 \times 10^{44}$ ergs s^{-1} (Table 1). These 10 clusters were imaged with the Advanced Camera for Surveys (ACS) Wide Field Channel (WFC) on *HST* during Cycle 12 (GO project 9722). Each cluster was imaged for two orbits (4.5 ks) through both the F555W (V_{555}) and F814W (I_{814}) filters. These data were retrieved from the STScI archive and reduced using standard STScI software (MultiDrizzle ver. 2.7) to provide final images with 0.05″ sampling and good cosmetic properties.

We extracted the photometry from the ACS images using SExtractor (Bertin & Arnouts 1996) run in dual-image mode so that photometric information from the V_{555} band was extracted for all sources detected on the I_{814}-band image and ensuring that we have precise aperture photometry for even crowded sources. Throughout this paper we use 1.4″ apertures (9 kpc diameter) to

calculate the ($V_{555} - I_{814}$) color, and the "best" magnitude is used for the total I_{814}-band magnitude [these correspond closely to rest-frame ($U - V$) colors and V absolute magnitudes].

The low-redshift, $z \sim 0.1$, comparison sample for our analysis comes from the Las Campanas/AAT Rich Cluster Survey (LARCS; Pimbblet et al. 2001, 2006). This survey obtained panoramic, ground-based B- and R-band imaging of 10 X-ray luminous ($L_X > 5 \times 10^{44}$ ergs s^{-1}) clusters at $z = 0.08$–0.15 selected from the *ROSAT* All-Sky Survey (Table 1). The observations and their reduction and analysis are described in detail in Pimbblet et al. (2001). Here we use 4″ ($B - R$) colors [corresponding to rest-frame ($U - V$) colors in 9 kpc apertures] and total magnitudes derived from these rest-frame $\sim V$-band-selected galaxy catalogs in our analysis. These data are thus well matched to the observations of the distant sample: the absolute V-band surface brightness limits are $\mu_V = -15.4$ and -15.8 mag arcsec^{-2} for LARCS and MACS, respectively, with spatial resolution of 2.8 and 1.0 kpc. In our analysis we only consider the inner parts of each cluster, within a radius of 600 kpc of the cluster center as identified from the X-ray emission (usually corresponding to the position of the brightest

cluster galaxy) as this provides uniform coverage across both the LARCS and MACS data sets.

Both the MACS and LARCS cluster samples were selected from the same X-ray survey, and the luminosities for the clusters are sufficiently bright that they should correspond to some of the most extreme environments at their respective epochs. The median X-ray luminosities of the high- and low-redshift samples are 17.0 and 7.3×10^{44} ergs s^{-1}, respectively, corresponding to a difference of less than a factor of 2 in the typical total mass (Reiprich & Boehringer 2002). However, an important issue to address is that the mass of the $z \sim 0.5$ progenitors of the LARCS clusters would be even lower than the MACS clusters. Using the results of Tormen (1998), we see that the progenitors of the LARCS clusters at $z \sim 0.5$ would be ∼3.5 times less massive than the MACS sample (with corresponding X-ray luminosities of ∼2×10^{44} ergs s^{-1}; Reiprich & Boehringer 2002). There is no evidence for strong variations in the galaxy luminosity function between clusters spanning such a relatively modest difference in typical mass (de Propris et al. 1999). In addition, Wake et al. (2005) see no variation in the blue galaxy fraction in clusters covering a similar range in mass. Combining these two results, we therefore expect that any differences between the galaxy populations in these two samples will primarily reflect evolutionary differences between $z \sim 0.5$ and $z \sim 0.1$.

Finally, to better define the evolutionary trends we are searching for, we also include similar observations of seven additional clusters in our analysis of the dwarf-giant ratio in § 3.3. We include a low-redshift point from U- and V-band observations of the Coma Cluster from a data set of known members (Godwin et al. 1983). This is well matched to our main MACS and LARCS samples. Next, we include four additional clusters that are at redshifts intermediate between the LARCS and MACS samples and a further two clusters at redshift beyond the MACS sample (see Table 1). These clusters all have deep archival observations with *HST* in the F555W/F606W and F814W filters (from GO projects 9033, 9290, 9722, 10325, 10491, 10872, and 10875), and we obtain the data from the *HST* archive. We note that the *HST* ACS observations of the four intermediate clusters do not reach the 600 kpc radius adopted for our analysis and so we have corrected the dwarf-giant ratio using the average observed radial trend in this ratio for the composite MACS sample. The dwarf-giant ratio is observed to increase in value from the cluster center outwards and flatten at larger radii. For the most extreme case, cluster Abell 1703 at $z = 0.258$, this correction gives an enhancement of 15% in dwarf-giant ratio. In addition we caution that the K-corrections for the additional *HST* clusters are not as well matched to rest-frame ($U - V$) as those for the LARCS or MACS samples and so there may be systematic uncertainties related to these data points.

3. ANALYSIS AND DISCUSSION

We show in Figure 1 the color-magnitude diagrams for the individual MACS $z \sim 0.5$ clusters (similar plots for the individual LARCS clusters are given in Pimbblet et al. 2002). These display strong linear features in the distributions of the brighter and redder galaxies in the fields. These are the color-magnitude relations for the passive, early-type cluster members (Sandage & Visvanathan 1978; Bower et al. 1992). For the brighter galaxies in the clusters this sequence is thought to represent variations in the metallicity and to a lesser extent age of the stellar populations in the galaxies (Kodama & Arimoto 1997; Terlevich et al. 2001).

As our MACS and LARCS cluster samples are homogeneously selected and observed and cover a small range in redshift

($\sigma z/z \sim 0.15$), we are able to combine them to reduce the influence of variations in field contamination and to improve the statistics of our analysis. We show in the two lower panels of Figure 1 the combined color-magnitude relations for the MACS and LARCS samples. The combined color-magnitude plots were created by correcting the data to the median redshifts of the MACS and LARCS samples, $z = 0.54$ and $z = 0.13$, respectively, using the K-corrections from a Bruzual & Charlot (2003) solar metallicity, simple stellar population, $z_f = 5$ model and the appropriate distance modulae. We also define limits to the color-magnitude relation in these combined samples to allow us to quantitatively compare them. We define the limits on the basis of an error-weighted two-parameter fit to the slope of the combined MACS red sequence with a stripe width of 0.75 mag to include the observed scatter. The corresponding boundaries for the LARCS red sequence are then determined by K-correcting and color-converting the limits from the MACS sample using Bruzual & Charlot (2003) and the formulae given in Skiff (2003) and Natali et al. (1994). A correction for the observed change in red-sequence slope between the two epochs is also included by using the gradient found from error-weighted fitting to the combined LARCS red sequence. We plot on Figure 1 the corresponding color boundaries for the two samples. It is these red sequences that are used below to estimate the combined red-sequence luminosity functions and the relevant field correction.

3.1. *Field Correction*

The removal of field galaxies from our samples is crucial to provide a clean measurement of the cluster luminosity function. For the MACS *HST* sample we used blank fields from the Great Observatories Origins Deep Survey North (GOODS; Giavalisco et al. 2004). These provide estimates of the correction for field contamination in each bin in our color-selected luminosity functions. The variation in this correction between independent 16 arcmin^2 subregions of the 112 arcmin^2 blank field is included in the luminosity function errors. The correction for field contamination for the ground-based observations of the LARCS sample is calculated in a similar way. Here, however, we make use of the fact that the panoramic, $2°$ diameter, imaging of these clusters extends into the field population surrounding the clusters and so we can use the outskirts of the images to determine the field contamination. These estimates have been shown to be robust by Pimbblet et al. (2002). Again we determine the reliability of our field corrections by dividing the total 4600 arcmin^2 field region into 290 arcmin^2 subregions and determining the scatter in these independent areas. These field subregions are on scales comparable to the regions of the MACS and LARCS clusters we analyze. The typical 1 σ errors for the field correction are in the region of 10% for MACS and 20% for LARCS. We propagate these uncertainties through our entire analysis.

An additional source of contamination comes from higher redshift galaxies that have been gravitationally lensed by our clusters. This would effectively alter the field contamination in our sample, either increasing or decreasing it depending on the slope of the number counts (Taylor et al. 1998). To estimate the scale of this effect we compare the number counts of galaxies on the color-magnitude plane which are just redward of the cluster's color-magnitude sequence (and hence should be at higher redshifts) to similar regions of the color-magnitude plane for the blank fields. This provides an estimate of the potential enhancement in the surface density of red galaxies in the cluster centers due to lensing of ∼0.1%. Although only a very small effect, we include this factor in the field correction.
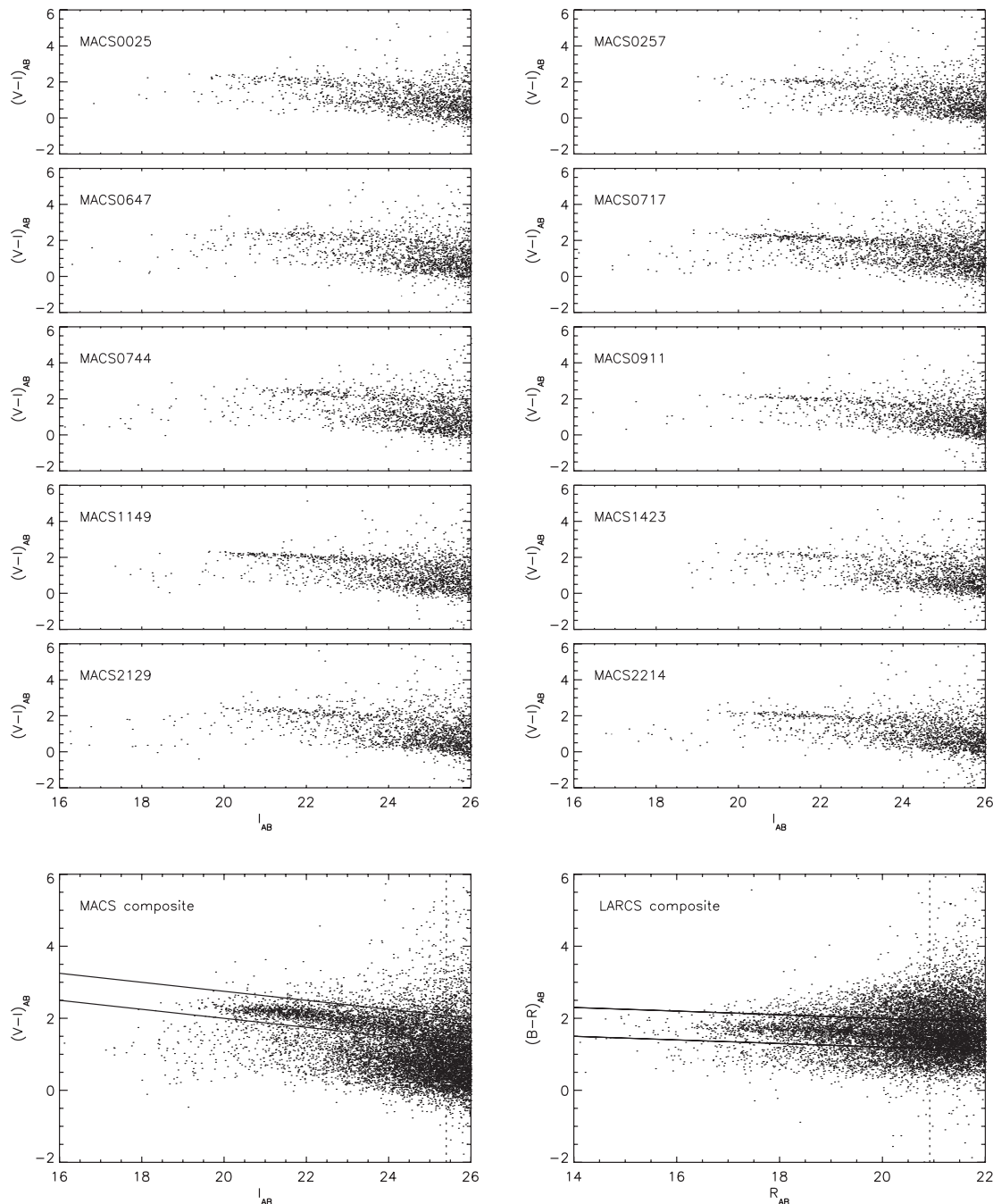
Fig. 1.—*Top 10 panels:* The individual ($V_{555} - I_{814}$) color-magnitude diagrams for the MACS clusters. *Bottom left panel:* The combined color-magnitude diagram for the MACS sample [corresponding to rest-frame $(U - V) - V$], all clusters have been K-corrected to $z = 0.54$. The solid lines show the limits used to define and select the red sequence in the combined clusters, and the dotted line is the 5 σ limit $I = 25.4$. *Bottom right panel:* The combined $(B - R) - R$ [rest-frame $(U - V) - V$] color-magnitude diagram for the LARCS sample. The dotted line denotes the 5 σ limit of $R = 20.92$ and all clusters have been K-corrected to $z = 0.13$. Again the solid lines show the limits used to select the red sequence in the combined clusters; these are transformed from the equivalent boundaries for the MACS sample as described in the text. Color-magnitude plots for individual clusters in the LARCS survey can be found in Pimbblet et al. (2002).

3.2. *Luminosity Function*

The field-corrected luminosity functions for the two composite cluster samples are shown in Figure 2. Luminosity functions are traditionally fitted with a single Schechter function (Schechter 1976). Recent papers on clusters, however, have instead fitted a Gaussian to the bright end of the luminosity function and a Schechter function to the faint end as these give a better fit to observations (Thompson & Gregory 1993; Dahlen et al. 2004). We compare the single Schechter to the Gaussian+Schechter

parameterization of the luminosity function for galaxies on the red sequences in the LARCS and MACS samples. To avoid incompleteness we only consider the luminosity function down to the K-corrected 5 σ limit of the highest redshift cluster in the shallower LARCS data ($R = 20.92$ from Abell 3888 corresponding to $M_V = -17.75$). Table 2 contains the best-fit Schechter and Gaussian parameters converted to absolute V-band magnitudes using the method described above and the reduced χ^2 for these fits. The errors quoted here are estimated using a bootstrap method.
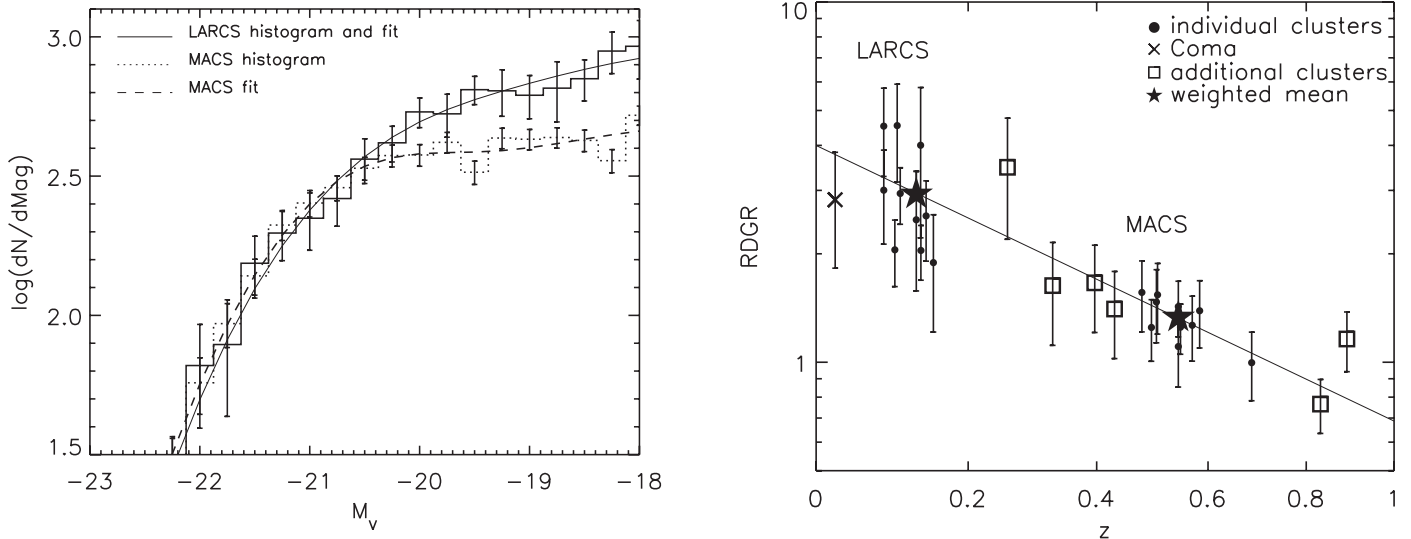
FIG. 2.—*Left:* The luminosity functions in the rest-frame V band for the red-sequence galaxies in the combined MACS and LARCS samples (normalized to the bright end of the LARCS sample). We plot the background-corrected data and our best-fit Gaussian+Schechter function fits. The errors are a combination of the Poisson uncertainty and the field correction error. Note the excess of faint red galaxies in the lower redshift LARCS sample, compared to the more distant MACS sample. *Right:* The variation in the red sequence RDGR with redshift for clusters in our two samples within 600 kpc of the cluster center and brighter than $M_V = -17.75$. We also plot the weighted mean values for each of the MACS and LARCS sample. A fit of the form $(1 + z)^{-\beta}$ to the MACS and LARCS points is plotted and yields $\beta = 2.5 \pm 0.5$. For comparison we show the equivalent measures for six additional high-redshift clusters and Coma (RDGR $= 2.8 \pm 1$), which follow the same trend.

When fitting combined Gaussian+Schechter functions we fix the mean magnitude and width of the Gaussian components (Table 2), within their errors, so as to constrain the evolution of the bright-end Gaussian between $z \sim 0.5$ and $z \sim 0.1$. We do this as the luminosity evolution of galaxies in the bright end of the LF is well constrained from fundamental plane studies (van Dokkum et al. 1998) and so we can focus on changes in the faint end. The passive evolution of the luminosity between the two epochs is fixed as 0.3 mag from van Dokkum & Franx (2001).

We find that both a Gaussian+Schechter or a Schechter function give acceptable fits to our two samples. Both parametric forms also demonstrate the same difference between the two samples: an increase in the number of faint red galaxies compared to the brighter red population at lower redshifts. For the Schechter fits this is shown by the steeper faint-end slope (α) in the LARCS clusters than MACS clusters, -1.11 ± 0.06 versus -0.91 ± 0.02, respectively, a difference of approximately 3.2 σ. We find no evidence for variations of the form of the luminosity function looking at either the bluest or reddest halves of the color-magnitude sequence or between different clusters when ranked by richness.

For the Gaussian+Schechter fits, the change in the luminosity function is shown in part by the relative normalization of the faint Schechter and bright Gaussian components, ϕ^*/amplitude, which decreases from 1.94 ± 0.58 in LARCS to 1.26 ± 0.67 for the MACS sample. However, the covariance between the param-

eters in the two components' functional fits makes such a comparison complex to interpret and so we turn to another, shape-independent, parameterization of the relative numbers of faint and luminous galaxies: the dwarf-giant ratio.

3.3. *Dwarf-Giant Ratio*

The results from § 3.2 are difficult to interpret in part because the form of the luminosity function is complex and its evolution is uncertain. A far simpler approach to quantify the relative evolution of the numbers of bright and faint galaxies is to use the ratio of the number of dwarfs to giants along the red sequence: the dwarf-giant ratio (DGR), which provides a single number to parameterize the distribution of galaxy luminosities within a population. The variation of this quantity (or its inverse GDR) with distance from cluster center, density, and cluster richness have been studied by a number of workers (Driver et al. 1998; Dahlen et al. 2004; Goto et al. 2005). Therefore, to provide a shape-independent comparison of the red galaxy populations in the MACS and LARCS clusters, we have measured the DGR.

The boundary between giants and dwarfs is arbitrary and is usually defined as the magnitude where the faint-end Schechter function begins to dominate over the bright-end Gaussian (Goto et al. 2005). Looking at the distributions in Figure 2, we therefore choose an absolute magnitude of $M_V \sim -19.9$ at $z = 0.13$ as our dividing point. This absolute magnitude brightens to $M_V \sim -20.2$ at $z = 0.54$ as we take into account the passive

TABLE 2

THE BEST-FITTING PARAMETERS FOR THE LUMINOSITY FUNCTION OF RED-SEQUENCE GALAXIES FOR THE MACS AND LARCS CLUSTERS

		SCHECHTER			GAUSSIAN [a]		
SURVEY	χ^2/ν	α	M_V^*	ϕ^*	$\langle M_V \rangle$	σ_M	Amplitude
LARCS.....................................	0.28	-1.11 ± 0.05	-21.10 ± 0.11	177.7 ± 22.2	...	...	...
	0.38	-0.92 ± 0.14	-19.43 ± 0.17	331.6 ± 57.2	-20.39 ± 0.12	0.89 ± 0.05	170.5 ± 21.8
MACS	1.29	-0.91 ± 0.02	-21.39 ± 0.05	215.1 ± 10.9	...	...	...
	1.14	-0.94 ± 0.19	-20.08 ± 0.67	223.0 ± 75.4	-20.86 ± 0.16	0.83 ± 0.08	177.2 ± 33.9

[a] Where the Gaussian fit parameters are not given this is a purely Schechter function fit to the luminosity function.

evolution models of van Dokkum & Franx (2001) (we have confirmed that our results are not sensitive to applying this factor). To ensure that our measurements of the DGR in the different samples are not affected by incompleteness, we adopt the same faint-end limit as for fitting the luminosity functions ($M_V \sim -17.75$) and as in § 3.2 we only consider galaxies within a 600 kpc radius of the center of each cluster. The limits chosen for our DGR analysis are comparable to those of De Lucia et al. (2004).

Figure 2 shows the variation of the DGR on the red sequence (RDGR) with redshift. The RDGR increases with cosmic time, and we attribute this to an increasing number of dwarfs on the red sequence. We determine weighted mean RDGRs for the MACS sample of 1.33 ± 0.06 and 2.93 ± 0.45 for LARCS, a difference of $3.7\,\sigma$. This corresponds to an increase in RDGR of a factor of 2.2 ± 0.4 from $z = 0.54$ to $z = 0.13$, or a look-back interval of 4 Gyr. An alternative way to look at this evolution is the variation in the proportion of integrated red light at the faint-end of the color-magnitude relation, which increases by a factor of 1.46 ± 0.14 from $z = 0.54$ to $z = 0.13$. This means that the stellar mass in the passive dwarf population ($M_V \lesssim -20$) now almost equals that in luminous cluster galaxies, whereas at $z \sim 0.5$ the giants dominated the total V-band luminosity from galaxies on the color-magnitude relation. The errors shown are a combination of the Poisson uncertainty and the field correction error.

We note that the LARCS RDGR errors are larger than those for MACS mainly due to the fact that at $z \sim 0.1$ the field galaxies and the faint end of the red sequence occupy the same region of $(B - R) - R$ color-magnitude space increasing the field correction error at the faint end (see Fig. 1). In contrast, the faint red sequence in the MACS sample at $z \sim 0.5$ is much easier to distinguish from the field using V and I bands.

To parameterize the evolution in the RDGR we fit a $(1 + z)^{-\beta}$ power law to the LARCS and MACS samples in Figure 2. We see that this provides a good description of the evolution for $\beta = 2.5 \pm 0.5$, with all of the clusters consistent with the fit. This confirms that the luminosity function of the red sequence in the central regions of massive clusters appears uniform with no clear evidence from our study of real cluster-to-cluster variations although the errors on individual clusters are large. We also find that the six additional clusters and Coma (RDGR = 2.8 ± 1) follow the same trend defined by the MACS and LARCS samples. De Lucia et al. (2004), who use a similar definition of DGR, found a value of 1.23 for clusters at $z = 0.75$ and a value of 2.9 for Coma, which are in good agreement with the trend we observe. The trend is also in qualitative agreement with the work of Kodama et al. (2004).

4. CONCLUSIONS

Our analysis of the red galaxy populations in X-ray-luminous clusters shows clear differences in the form of the luminosity function over the redshift range $z = 0.1$–0.5. These changes reflect an increase in the proportion of dwarf to giant galaxies in the population since $z \sim 0.5$, which we attribute to an increase in the number of dwarfs on the red sequence. We quantify this evolution using the shape-independent estimate of the relative evolution of the faint end of the luminosity function, the red-sequence dwarf-giant ratio (RDGR), which shows an increase

by a factor of 2.2 ± 0.4 between $z = 0.54$ and $z = 0.13$. This is equivalent to an increase of 1.46 ± 0.14 in the relative V-band luminosity (or stellar mass) in faint red galaxies with $M_V \lesssim -20$ compared to brighter systems over this period. This increase means that in local clusters, the luminosity contributed by giant and dwarf galaxies is comparable, whereas at $z = 0.5$ the giants were the dominant population on the color-magnitude relation.

Our results show that there is significant evolution since $z \sim 0.5$ in the faint, passive galaxy population in a well-defined sample of X-ray-luminous clusters. This agrees with the early results from De Lucia et al. (2004) and Kodama et al. (2004) on red galaxies in a more diverse range of structures. However, this is in disagreement with the work of Andreon (2006), who sees no such evolution. This disagreement may be simply due to Andreon's use of a single cluster, as our analysis shows a large cluster-to-cluster scatter, but with large errors (due to an uncertain field correction). We conclude that a large proportion of the passive galaxy population at the faint end of the color-magnitude sequence in local clusters either did not reside in similar, high-density environments 5 Gyr ago (at $z \sim 0.5$), or, if they were present in these regions, had significantly bluer colors (suggesting that they were actively star-forming) and so do not fall within the color-magnitude relation.

Clusters in the mass range studied in this work are expected to have roughly doubled their masses since $z \sim 0.5$ (Tormen 1998), and hence many of the faint red galaxies (or at least their progenitors) may have arrived in the core regions of the cluster between $z \sim 0.5$ and $z \sim 0.1$. However, we believe that the major driver of the evolution we see is the transformation of blue, star-forming galaxies into passive, red systems that lie on the color-magnitude relation. If correct, this suggests that there will be an increasing diversity in the star formation histories of passive galaxies at $M_V \lesssim -20$ in intermediate-redshift clusters (at $z \sim 0.3$–0.4), and studies of age-sensitive indicators at these depths may uncover evidence for recent star formation activity within these galaxies (e.g., Smail et al. 2001).

We end by noting that studies such as this one can be extended to a wider range of environments and redshifts out to $z \sim 1$ using the data from the UKIRT Infrared Deep Sky Survey (UKIDSS; Lawrence et al. 2007) in concert with the *XMM-Newton* Large Scale Structure Survey (*XMM* LSS). Such studies will allow the evolution of the passive population on the color-magnitude relation and its build-up to be tracked as a function of environment and epoch, and will demonstrate the importance of including environmental effects when modeling the color-magnitude relation in galaxy evolution models.

REFERENCES

Andreon, S. 2006, MNRAS, 369, 969
Aragon-Salamanca, A., Ellis, R. S., Couch, W. J., & Carter, D. 1993, MNRAS, 262, 764
Baldry, I. K., Balogh, M. L., Bower, R. G., Glazebrook, K., Nichol, R. C., Bamford, S. P., & Budavari, T. 2006, MNRAS, 373, 469

Bertin, E., & Arnouts, S. 1996, A&AS, 117, 393
Bower, R. G., Lucey, J. R., & Ellis, R. S. 1992, MNRAS, 254, 589
Bruzual, G., & Charlot, S. 2003, MNRAS, 344, 1000
Dahlen, T., Fransson, C., Ostlin, G., & Naslund, M. 2004, MNRAS, 350, 253
De Lucia, G., et al. 2004, ApJ, 610, L77

De Lucia, G., et al. 2007, MNRAS, 374, 809
de Propris, R., Stanford, S. A., Eisenhardt, P. R., Dickinson, M., & Elston, R. 1999, AJ, 118, 719
Dressler, A., et al. 1997, ApJ, 490, 577
Driver, S. P., Couch, W. J., & Phillipps, S. 1998, MNRAS, 301, 369
Ebling, H., Barrett, E., Donovan, D., Ma, C.-J., Edge, A. C., & van Speybroeck, L. 2007, ApJ, 661, L33
Ebeling, H., Edge, A. C., & Henry, J. P. 2001, ApJ, 553, 668
Ferguson, H. C., & Binggeli, B. 1994, A&A Rev., 6, 67
Giavalisco, M., et al. 2004, ApJ, 600, L93
Godwin, J. G., Metcalfe, N., & Peach, J. V. 1983, MNRAS, 202, 113
Goto, T., et al. 2005, ApJ, 621, 188
Grebel, E. K. 1999, in IAU Symp. 192, The Stellar Content of Local Group Galaxies, ed., P. Whitelock & R. Cannon (San Francisco: ASP), 17
Hogg, D. W., et al. 2004, ApJ, 601, L29
Kodama, T., & Arimoto, N. 1997, A&A, 320, 41
Kodama, T., et al. 2004, MNRAS, 350, 1005
Lawrence, A., et al. 2007, MNRAS, in press (astro-ph/0604426)
Natali, F., Natali, G., Pompei, E., & Pedichini, F. 1994, A&A, 289, 756
Pimbblet, K. A., Smail, I., Edge, A. C., Couch, W. J., O'Hely, E., & Zabludoff, A. I. 2001, MNRAS, 327, 588
Pimbblet, K. A., Smail, I., Edge, A. C., O'Hely, E., Couch, W. J., & Zabludoff, A. I. 2006, MNRAS, 366, 645
Pimbblet, K. A., Smail, I., Kodama, T., Couch, W. J., Edge, A. C., Zabludoff, A. I., & O'Hely, E. 2002, MNRAS, 331, 333
Poggianti, B. M., et al. 2001, ApJ, 562, 689
Reiprich, T. H., & Boehringer, H. 2002, ApJ, 567, 716
Sandage, A., & Visvanathan, N. 1978, ApJ, 225, 742
Schechter, P. 1976, ApJ, 203, 297
Skiff, A. B. 2003, LONEOS Catalog, ver. 2003 July 15 (Flagstaff: Lowell: Obs.), ftp://ftp.lowell.edu/pub/bas/starcats
Smail, I., Kuntschner, H., Kodama, T., Smith, G., Packham, C., Fruchter, A., & Hook, R. 2001, MNRAS, 323, 839
Stanford, S. A., Eisenhardt, P. R., & Dickinson, M. 1998, ApJ, 492, 461
Taylor, A. N., Dye, S., Broadhurst, T. J., Benitez, N., & van Kampen, E. 1998, MNRAS, 501, 539
Terlevich, A. I., Caldwell, N., & Bower, R. G. 2001, MNRAS, 326, 1547
Thompson, L. A., & Gregory, S. A. 1993, AJ, 106, 2197
Tormen, G. 1998, MNRAS, 297, 648
van Dokkum, P., & Franx, M. 2001, ApJ, 553, 90
van Dokkum, P. G., Franx, M., Kelson, D. D., & Illingworth, G. D. 1998, ApJ, 504, L17
Wake, D. A., Collins, C. A., Nichol, R. C., Jones, L. R., & Burke, D. J. 2005, ApJ, 627, 186